Electromagnetic propagation in close-packed disordered suspensions

V. A. Davis
Physics Department, Brandeis University, Waltham, Massachusetts 02254

L. Schwartz
Schlumberger-Doll Research, Old Quarry Road, Ridgefield, Connecticut 06877-4108

(Received 23 October 1984)

Multiple-scattering theory is used to evaluate the effective dielectric function $\epsilon(\omega)$ for disordered systems in which spherical inclusions are densely packed in a host medium. We compare the well-known quasicrystalline approximation (QCA) with Roth's effective-medium approximation (EMA). Both approaches are studied in the long-wavelength limit and, also, in the regime where the wavelength and particle diameter are comparable. In the long-wavelength case, the QCA reduces to the elementary Maxwell-Garnett formula. By contrast, the EMA is shown to include the effects of local-field fluctuations. The QCA and EMA are applied to two situations of experimental interest: (1) a strong-scattering system comprised of metal spheres embedded in a KCl matrix, and (2) a weak-scattering system made of pressed Al_2O_3 particles. In both cases there are significant differences between the two approximation schemes and the EMA is generally to be preferred.

I. INTRODUCTION

The description of electromagnetic propagation in two-component disordered materials in terms of the properties of the constituents is a problem with a long history. Recent interest in the technological properties[1] of these systems has led to renewed experimental[2–8] and theoretical[9–18] study of this classic problem.

In this paper we are concerned with composites whose microgeometry is that of a suspension. In suspensions only one of the two components (the host) forms percolating paths through the system. The other component is present in the form of nonoverlapping grains. Having assumed this geometry, the propagation of electromagnetic waves can be described within the framework of multiple-scattering theory.[12–14,16–18] For simplicity, we will assume that all the inclusions are spheres of the same radii. (This last assumption implies that the relative packing fraction η of the inclusions is limited to the range $0<\eta<0.62$.) In multiple-scattering theory the wave interacts with a sequence of isolated scattering centers, and the effective dielectric function of the composite is obtained by averaging over the allowed configurations of the system. The advantage of this approach is that the formulation of the central equations does not require any assumptions regarding either the magnitude of the packing fraction[19] or the strength of the scattering. Of course, if neither of these parameters is small, considerable care must be taken in developing suitable approximation schemes.

The theoretical description of disordered composites usually proceeds in terms of three distinct mean-field theories, all of which can be understood in terms of basic multiple-scattering theory. These are the average-t-matrix approximation[20] (ATA), the coherent-potential approximation[21] (CPA), and the iterated dilute approximation[22] (IDA). The ATA is also known as the Maxwell-Garnett or Clausius-Mossotti approximation,[23] and the CPA is often referred to as the effective-medium approximation (EMA). (Here, we use the less familiar name, CPA, to avoid confusion with an entirely different EMA to be discussed below.) The IDA, which is sometimes refered to as the self-similar approximation, is based on successive applications of either the ATA or the CPA. (As both approximations are correct in the dilute limit,[13] either can be used to generate the IDA.) The equations defining these approximations are the following:

$$\frac{\epsilon_{\rm eff}}{\epsilon_0}=1+\frac{3\eta[(\epsilon_s-\epsilon_0)/(2\epsilon_0+\epsilon_s)]}{1-\eta[(\epsilon_s-\epsilon_0)/(2\epsilon_0+\epsilon_s)]} \quad \text{for the ATA}, \tag{1}$$

$$\eta\frac{\epsilon_s-\epsilon_{\rm eff}}{2\epsilon_{\rm eff}+\epsilon_s}+(1-\eta)\frac{\epsilon_0-\epsilon_{\rm eff}}{2\epsilon_{\rm eff}+\epsilon_0}=0 \quad \text{for the CPA}, \tag{2}$$

and

$$\int_{\epsilon_0}^{\epsilon_{\rm eff}}\frac{d\epsilon}{3\epsilon}\frac{2\epsilon+\epsilon_s}{\epsilon_s-\epsilon}=-\int_1^{1-\eta}\frac{d\phi}{\phi} \rightarrow\left[\frac{\epsilon_s-\epsilon_{\rm eff}}{\epsilon_s-\epsilon_0}\right]\left[\frac{\epsilon_0}{\epsilon_{\rm eff}}\right]^{1/3} =1-\eta \quad \text{for the IDA}. \tag{3}$$

Here, $\epsilon_0(\omega)$ and $\epsilon_s(\omega)$ are the dielectric functions for the host and inclusions, respectively, and $\epsilon_{\rm eff}(\omega)$ is the corresponding effective dielectric function for the composite. [In general, all of these quantities may be frequency (ω) dependent.] The ATA, CPA, and IDA are to be used under different circumstance. The ATA and IDA are appropriate in a suspension geometry, while the CPA is applicable when the two components are interspersed on an equal footing.[13] Nevertheless, there are important simi-

larities between these approximations: (1) they are all long-wavelength approximations, (2) they all describe scattering processes within the dipole approximation, and (3) the only information about the structure of the system which enters these approximations is the packing fraction η, i.e., none of them make use of higher-order density-correlation functions. Regarding point (1) we note that there are systems of experimental interest in which the wavelength of the radiation is comparable to the size of the individual grains.[7] In connection with point (2), several authors have stressed the importance of including higher multipoles in an accurate calculation of the *long-wavelength* properties of composite systems.[11,13] [At higher frequencies, classical arguments imply that multipoles up to $j_{\max}\sim\frac{1}{2}kd$ must be included (here, k is the host wave vector and d is a typical particle diameter).] Finally, over the entire frequency range, it is natural to ask how information regarding density-correlation functions can be included in a calculation of $\epsilon_{\text{eff}}(\omega)$.

Previous efforts to address these questions within multiple-scattering theory have focused on the application of Lax's quasicrystalline approximation (QCA).[12–14,24] The QCA is a reasonable approximation on physical grounds and has the advantage that it can be applied in a straightforward manner to a variety of physical systems. We have found, however, that the effective-medium approximation[25–27] (EMA) developed by Roth has several important advantages over the QCA. (The application of the EMA to the calculation of electrical conductivity in a related class of disordered systems has been discussed in Ref. 9.) This is particularly evident in systems with a high density of strong scatterers, as is often the case when metal particles are embedded in an insulating matrix.[2–6,8,16] Here, the EMA leads to a more realistic description of the structure in both the real and imaginary parts of $\epsilon_{\text{eff}}(\omega)$. (This is analogous to the situation encountered in calculating the electronic properties of liquid and amorphous metals with resonant d bands.[25,26]) In the long-wavelength limit there are also important distinctions between the EMA and QCA. In this limit it can be shown that the QCA reduces to the ATA result of Eq. (1).[14] By contrast, we show that, as $kd\to 0$, the EMA dielectric function depends on contributions from the pair-distribution function $g(R)$ and higher-multipole terms in the single-sphere scattering matrix. Thus the EMA is the only available theory of structurally disordered systems which includes proximity effects in the calculation of $\epsilon_{\text{eff}}(\omega)$.

In Sec. II the general equations of multiple-scattering theory are reviewed briefly and the QCA and EMA prescriptions for evaluating $\epsilon_{\text{eff}}(\omega)$ are formulated. We also discuss the limiting form of these equations as $kd\to 0$ and show that the form predicted by the EMA is reasonable on physical grounds.[28] In Sec. III the application of these approximations to two experimental situations is discussed. The first is a strong-scattering system of silver spheres embedded in potassium chloride. We examine the position and shape of the plasmon resonance and find that the EMA provides the most realistic description. The need for an adequate theory of these resonances has recently been emphasized by Leibsch and coworkers.[16] The second material is a close-packed weak-scattering system of Al_2O_3 pressed grains in air. In recent experimental work the dielectric function of this system has been studied over an extremely wide frequency range ($0.78<kd<94.25$). Unfortunately, the methods employed in the present paper can be used to describe only a small part of this range ($0.0<kd<3.5$). Within this limited regime, our calculations indicate that the EMA is in somewhat better agreement with the experimental results than the QCA. It is clear, however, that further work must be done before either approximation can be used efficiently over the entire frequency range covered in Ref. 7.

II. FORMALISM

A. General equations

In a given configuration of a disordered suspension and in the absence of external currents, the (vector) wave equation satisfied by the electric field is

$$\nabla\times\nabla\times\mathscr{E}(\mathbf{x})-k^2\epsilon(\mathbf{x},\omega)\mathscr{E}(\mathbf{x})=\mathbf{0}\ . \tag{4}$$

Here, $k^2=\epsilon_0(\omega)(\omega^2/c^2)$, and $\epsilon(\mathbf{x},\omega)$ is the scaled dielectric function equal to 1 for $\mathbf{x}$ in the host material and $\epsilon_s(\omega)/\epsilon_0(\omega)$ for $\mathbf{x}$ within the spheres. (Both the host and the inclusions are assumed to be nonmagnetic.) The (dyadic) equation for the *configuration-dependent* Green's function $\overleftrightarrow{\mathscr{G}}(\mathbf{x},\mathbf{x}')$ can be written either in differential form,

$$\nabla\times\nabla\times\overleftrightarrow{\mathscr{G}}(\mathbf{x},\mathbf{x}')-k^2\epsilon(\mathbf{x},\omega)\overleftrightarrow{\mathscr{G}}(\mathbf{x},\mathbf{x}')=\overleftrightarrow{\mathbb{I}}\delta(\mathbf{x}-\mathbf{x}')\ , \tag{5}$$

or as an integral equation,

$$\overleftrightarrow{\mathscr{G}}(\mathbf{x},\mathbf{x}')=\overleftrightarrow{G}_0(\mathbf{x}-\mathbf{x}')+\int d\mathbf{x}_1\,\overleftrightarrow{G}_0(\mathbf{x},\mathbf{x}_1)\cdot\epsilon(\mathbf{x}_1,\omega)\overleftrightarrow{\mathscr{G}}(\mathbf{x}_1,\mathbf{x}')\ . \tag{6}$$

[The host Green's function $\overleftrightarrow{G}_0(\mathbf{x}-\mathbf{x}')$ is defined by an equation identical to (5) in which $\epsilon(\mathbf{x},\omega)\to 1$.]

The physical properties of the system are determined by $\overleftrightarrow{G}(\mathbf{x}-\mathbf{x}')\equiv\langle\overleftrightarrow{\mathscr{G}}(\mathbf{x},\mathbf{x}')\rangle$, the average of $\overleftrightarrow{\mathscr{G}}(\mathbf{x},\mathbf{x}')$ over all allowed configurations of the suspension. This quantity can be written in terms of either the average total scattering operator $\overleftrightarrow{T}(\mathbf{x}-\mathbf{x}')$ or the self-energy $\overleftrightarrow{\Sigma}(\mathbf{x}-\mathbf{x}')$:

$$\overleftrightarrow{G}(\mathbf{x}-\mathbf{x}')=\overleftrightarrow{G}_0(\mathbf{x}-\mathbf{x}')+\int d\mathbf{x}_1\,d\mathbf{x}_2\,\overleftrightarrow{G}_0(\mathbf{x}-\mathbf{x}_1)\cdot\overleftrightarrow{T}(\mathbf{x}_1-\mathbf{x}_2)\cdot\overleftrightarrow{G}_0(\mathbf{x}_2-\mathbf{x}')\ , \tag{7a}$$

$$\overleftrightarrow{G}(\mathbf{x}-\mathbf{x}')=\overleftrightarrow{G}_0(\mathbf{x}-\mathbf{x}')+\int d\mathbf{x}_1\,d\mathbf{x}_2\,\overleftrightarrow{G}_0(\mathbf{x}-\mathbf{x}_1)\cdot\overleftrightarrow{\Sigma}(\mathbf{x}_1-\mathbf{x}_2)\cdot\overleftrightarrow{G}(\mathbf{x}_2-\mathbf{x}')\ . \tag{7b}$$

Because the average system is translationally invariant, it is convenient to transform the above equations to the momentum representation. Equations (7) can then be rewritten as

$$\overleftrightarrow{G}(p)=\overleftrightarrow{G}_0(p)+\overleftrightarrow{G}_0(p)\cdot\overleftrightarrow{T}(p)\cdot\overleftrightarrow{G}_0(p)\ , \tag{8a}$$

$$\overleftrightarrow{G}(p)=\overleftrightarrow{G}_0(p)+\overleftrightarrow{G}_0(p)\cdot\overleftrightarrow{\Sigma}(p)\cdot\overleftrightarrow{G}(p)=\{[\overleftrightarrow{G}_0(p)]^{-1}-\overleftrightarrow{\Sigma}(p)\}^{-1}\ . \tag{8b}$$

To compute the effective dielectric function $\epsilon_{\text{eff}}(\omega)$, we recall that the wave-vector—versus—frequency relation governing wave propagation in a disordered system is determined by the *singularities* of the average Green's function in the (p,ω) plane.[12,14] [It is clear from Eq. (8a) that the singularities of $\overleftrightarrow{G}(p)$ and $\overleftrightarrow{T}(p)$ are identical.] In other words, for each ω we find the value of $p \equiv p_{\text{eff}}(\omega)$ that leads to a singularity in the transverse part of $\overleftrightarrow{G}(p)$.[29] Once $p_{\text{eff}}(\omega)$ is known, we have $\epsilon_{\text{eff}}(\omega) \equiv k^{-2} p_{\text{eff}}^2(\omega)$, or alternatively,

$$\epsilon_{\text{eff}}(\omega) = 1 + \Sigma_\perp(p_{\text{eff}}(\omega))/k^2 \ . \tag{9}$$

[Thus, if we are interested only in the dispersion relation, we can work with an effective dielectric function that depends on just the frequency and avoid dealing with momentum-dependent quantities like $\overleftrightarrow{\Sigma}(p)$.] In general, the value of $p_{\text{eff}}(\omega)$ will be complex. In most cases of interest, however, the imaginary part of $p_{\text{eff}}(\omega)$ will be small compared to its real part and, rather than searching for poles in the complex plane, we can simply scan *real* p and look for peaks in the transverse part of $\overleftrightarrow{G}(p)$. The corresponding real value of p is then used in Eq. (9) to calculate $\epsilon_{\text{eff}}(\omega)$. This approach will provide an accurate description of the effective propagation as long as the imaginary part of $p_{\text{eff}}(\omega)$ is small and $\Sigma_\perp(p)$ is a smooth function in the region near the pole of $\overleftrightarrow{G}(p)$.

Within the framework of multiple-scattering theory, the quantity $\overleftrightarrow{T}(\mathbf{x}-\mathbf{x}')$ introduced in Eq. (7a) is obtained by averaging the *configuration-dependent* total scattering operator $\overleftrightarrow{\mathcal{T}}(\mathbf{x},\mathbf{x}')$. The latter quantity is most conveniently written as a series expansion in terms of the operators $\overleftrightarrow{t}_\alpha$ that describe scattering by a single inclusion centered at $\mathbf{R}_\alpha$:

$$\overleftrightarrow{\mathcal{T}} = \sum_\alpha \overleftrightarrow{t}_\alpha + \sum_{\substack{\alpha \\ \beta\neq\alpha}} \overleftrightarrow{t}_\alpha \cdot \overleftrightarrow{G}_0 \cdot \overleftrightarrow{t}_\beta + \sum_{\substack{\alpha \\ \beta\neq\alpha \\ \gamma\neq\beta}} \overleftrightarrow{t}_\alpha \cdot \overleftrightarrow{G}_0 \cdot \overleftrightarrow{t}_\beta \cdot \overleftrightarrow{G}_0 \cdot \overleftrightarrow{t}_\gamma + \sum_{\substack{\alpha \\ \beta\neq\alpha \\ \gamma\neq\beta \\ \delta\neq\gamma}} \overleftrightarrow{t}_\alpha \cdot \overleftrightarrow{G}_0 \cdot \overleftrightarrow{t}_\beta \cdot \overleftrightarrow{G}_0 \cdot \overleftrightarrow{t}_\gamma \cdot \overleftrightarrow{G}_0 \cdot \overleftrightarrow{t}_\delta + \cdots \ , \tag{10}$$

where the explicit dependence on $\mathbf{x}$, $\mathbf{x}_1, \ldots, \mathbf{x}'$ has been suppressed. Approximation schemes for computing the configuration average of this series are discussed below. Once $\overleftrightarrow{T}(p)$ is known, the self-energy can be evaluated as

$$\overleftrightarrow{\Sigma}(p) = \overleftrightarrow{T}(p)[\overleftrightarrow{\mathbb{1}} + \overleftrightarrow{G}_0 \cdot \overleftrightarrow{T}(p)]^{-1} \ , \tag{11}$$

and the calculation of $\epsilon_{\text{eff}}(\omega)$ is essentially straightforward.

B. Single-particle scattering

The Mie scattering operator $\overleftrightarrow{t}_\alpha(k)$ describes the interaction of an electromagnetic wave (with frequency $\omega = ck$) with an isolated grain centered at $\mathbf{R}_\alpha$. Because the grains are assumed to be spherical, the most convenient representation for these operators is in terms of vector spherical harmonics.[14] We use the following definitions:

$$\mathbf{Y}_{jm}^{(0)}(\hat{\mathbf{x}}) = \hat{\mathbf{r}}\, Y_{jm}(\hat{\mathbf{x}}) \ , \tag{12a}$$

$$\mathbf{Y}_{jm}^{(e)}(\hat{\mathbf{x}}) = \frac{1}{\sqrt{j(j+1)}} r \nabla Y_{jm}(\hat{\mathbf{x}}) \ , \tag{12b}$$

$$\mathbf{Y}_{jm}^{(m)}(\hat{\mathbf{x}}) = \frac{1}{\sqrt{j(j+1)}} \nabla \times [\mathbf{r} Y_{jm}(\hat{\mathbf{x}})] \ , \tag{12c}$$

where $Y_{jm}(\hat{\mathbf{x}})$ are the usual scalar spherical harmonics. To simplify our notation we adopt the composite indices $J=(j,m)$ and $L=(\lambda,J)$ (λ runs over the values o, e, and m). Suppressing the explicit dependence on k, the momentum-space matrix elements of $\overleftrightarrow{t}_\alpha$ can be written as

$$\langle \mathbf{p} | \overleftrightarrow{t}_\alpha | \mathbf{p}' \rangle = \frac{e^{i(\mathbf{p}'-\mathbf{p})\cdot\mathbf{R}_\alpha}}{\Omega} (4\pi)^2 \sum_{\substack{J, \\ \lambda,\lambda'}} \mathbf{Y}_J^\lambda(\hat{\mathbf{p}}) t_j^{\lambda\lambda'}(p,p') \mathbf{Y}_J^{\lambda'}(\hat{\mathbf{p}}') \ , \tag{13}$$

where Ω is the volume of the system. The structure of the matrix $t_j^{\lambda\lambda'}(p,p')$ is

$$t_j^{\lambda\lambda'}(p,p') = \begin{bmatrix} t_j^{oo}(p,p') & t_j^{oe}(p,p') & 0 \\ t_j^{eo}(p,p') & t_j^{ee}(p,p') & 0 \\ 0 & 0 & t_j^{mm}(p,p') \end{bmatrix} . \tag{14}$$

The elements of this matrix are given in detail in Ref. 14. Note that the only off-diagonal elements are $t_j^{eo}(p,p')$ and $t_j^{oe}(p,p')$. It can easily be shown that these quantities do not contribute to the transverse part of either $\overleftrightarrow{T}(p)$ or $\overleftrightarrow{G}(p)$. Accordingly, the Mie scattering operator can be treated as a vector indexed by $l=(\lambda,j)$ rather than as a dyad.

C. Approximate decoupling procedures

In dense suspensions there are important correlations between the average positions of the scattering centers. In practice, however, the available information is usually limited to the two-particle or pair distribution $g(R)$. [Given a grain centered at the origin, $g(R)$ gives the relative probability to find another grain centered a distance R away from the origin; $g(R)=0$ for R less than the grain diameter and $g(R)\to 1$ as $R\to\infty$.] In developing expressions for the average total-scattering operator, higher-order correlations must be described (approximately) in terms of $g(R)$. Two such decoupling schemes are the QCA (Refs. 12, 14, and 24) and the EMA (Refs. 25–28). [Previous calculations, all of which are based on the QCA, have estimated $g(R)$ with either the hole correction [$g(R)=0$ for $R<d$ and $g(R)=1$ for $R>d$] (Refs. 12 and 14) or the Percus-Yevick distribution (Refs. 14 and 17). The present calculations are based on a close-packed distribution which is somewhat smoother than the

Percus-Yevick $g(R)$ (Ref. 30).]

In both the QCA and EMA, T is written as an integral over all possible initial- and final-site indices:

$$T=\int d\mathbf{R}_\alpha d\mathbf{R}_{\alpha'}\, T(\alpha\,|\,\alpha')\ . \tag{15}$$

(Note that we have suppressed the explicit dyad notation.) In the QCA, $g(\,|\,\mathbf{R}_\alpha-\mathbf{R}_\beta\,|\,)\equiv g(\alpha\,|\,\beta)$ is used to correlate each pair of *consecutive* scatterings. This leads to an expression of the form:

$$\begin{aligned}T^{\mathrm{QCA}}(\alpha\,|\,\alpha')=&\,nt_\alpha\delta(\mathbf{R}_\alpha-\mathbf{R}_{\alpha'})+n^2t_\alpha g(\alpha\,|\,\alpha')G_0t_{\alpha'}\\&+n^3\int d\mathbf{R}_{\alpha_1}t_\alpha g(\alpha\,|\,\alpha_1)\\&\times G_0t_{\alpha_1}g(\alpha_1\,|\,\alpha')G_0t_{\alpha'}+\cdots\ ,\end{aligned} \tag{16}$$

where n is the number density of inclusions. A more sophisticated decoupling procedure is given by the EMA.[25–28] Here, T is described by a series similar in structure to (16), but in which the propagators and scattering operators are replaced by renormalized quantities:

$$\begin{aligned}T^{\mathrm{EMA}}(\alpha\,|\,\alpha')=&\,nT_\alpha\delta(\mathbf{R}_\alpha-\mathbf{R}_{\alpha'})+n^2T_\alpha\widetilde{G}(\alpha\,|\,\alpha')T_{\alpha'}\\&+n^3\int dR_{\alpha_1}T_\alpha\widetilde{G}(\alpha\,|\,\alpha_1)\\&\times T_{\alpha_1}\widetilde{G}(\alpha_1\,|\,\alpha')T_{\alpha'}+\cdots\ .\end{aligned} \tag{17}$$

T_α and $\widetilde{G}(\alpha\,|\,\alpha')$ are determined by the self-consistent equations

$$\begin{aligned}\widetilde{G}(\alpha\,|\,\alpha')=&\,g(\alpha\,|\,\alpha')G_0+h(\alpha\,|\,\alpha')\\&\times\int d\mathbf{R}_{\alpha_1}d\mathbf{R}_{\alpha_2}\widetilde{G}(\alpha\,|\,\alpha_1)T(\alpha_1\,|\,\alpha_2)\widetilde{G}(\alpha_2\,|\,\alpha')\ ,\end{aligned} \tag{18a}$$

where $h(\alpha\,|\,\alpha')\equiv g(\alpha\,|\,\alpha')-1$, and

$$T_\alpha=t_\alpha+t_\alpha G_0\int d\mathbf{R}_{\alpha_1}d\mathbf{R}_{\alpha_2}T(\alpha_1\,|\,\alpha_2)\widetilde{G}(\alpha_2\,|\,\alpha)T_\alpha\ . \tag{18b}$$

To compare the QCA and EMA, we consider the *exact* expansion of $T(\alpha\,|\,\alpha')$ in terms of G_0 and the Mie scattering operators.[25,28] Working through third order in the scattering strength, we have

$$\begin{aligned}T(\alpha\,|\,\alpha')=&\,nt_\alpha\delta(\mathbf{R}_\alpha-\mathbf{R}_{\alpha'})+n^2t_\alpha g(\alpha\,|\,\alpha')G_0t_{\alpha'}\\&+n^2\int d\mathbf{R}_{\alpha_1}t_\alpha g(\alpha\,|\,\alpha_1)G_0t_{\alpha_1}G_0t_\alpha\delta(\mathbf{R}_\alpha-\mathbf{R}_{\alpha'})\\&+n^3\int d\mathbf{R}_{\alpha_1}g(\alpha\,|\,\alpha_1\,|\,\alpha')t_\alpha G_0t_{\alpha_1}G_0t_{\alpha'}\ ,\end{aligned} \tag{19}$$

where $g(\alpha\,|\,\alpha_1\,|\,\alpha')$ is the normalized three-particle distribution function. The first two terms on the right-hand side of (19) are given correctly by both the QCA and EMA. Physically, the third term describes the repeated scattering sequence $\alpha\rightarrow\alpha_1\rightarrow\alpha$, while the fourth term describes the case in which α, α_1, and α' are all distinct. These last two terms illustrate the way in which the averaging of higher-order terms in the multiple-scattering series introduces *fluctuation* effects. In the EMA the structure of these two terms is reproduced within the Kirkwood approximation

$$g(\alpha\,|\,\alpha_1\,|\,\alpha')\rightarrow g(\alpha\,|\,\alpha_1)g(\alpha_1\,|\,\alpha')g(\alpha\,|\,\alpha')\ .$$

By contrast, within the QCA these two third-order processes are represented by a single term and no distinction regarding the first and last sites is made. It will be seen below that such distinctions are important in describing what are usually referred to as local-field fluctuations.[13,22,23,28]

In order to put the preceding *operator* equations in a form suitable for calculations, we work in the angular-momentum representation:[26]

$$\overleftrightarrow{\mathrm{T}}(p)=(4\pi)^2n\sum_{L,L'}\mathbf{Y}_L(\hat{\mathbf{p}})Q^{LL'}(\mathbf{p})\mathbf{Y}_{L'}(\hat{\mathbf{p}})\ . \tag{20}$$

Because $\mathbf{p}$ is on the z axis, the transverse part of $\overleftrightarrow{\mathrm{T}}$ comes only from the e and m parts of Q. It is easily seen that Q is diagonal in its azimuthal indices, so that we need only retain the $m=\pm1$ terms. Thus we can write

$$Q^{LL'}(\mathbf{p})=T_l(p,p)\delta_{LL'}+i^{j'-j}\frac{T_l(p,k)}{T_l}T_{LL'}(\mathbf{p})\frac{T_{l'}(k,p)}{T_{l'}} \tag{21a}$$

and

$$T_{LL'}(\mathbf{p})=T_l\{\widetilde{B}(\mathbf{p})[1-T\widetilde{B}(\mathbf{p})]^{-1}\}_{LL'}T_{l'}\ . \tag{21b}$$

where $T_l=T_l(k,k)$.

The QCA is obtained by substituting

$$T_l(p_1,p_2)\rightarrow t_l(p_1,p_2) \tag{22a}$$

and

$$\widetilde{B}_{LL'}(\mathbf{p})\rightarrow B_{LL'}(\mathbf{p})\ , \tag{22b}$$

where

$$B_{LL'}(\mathbf{p})=n\int d\mathbf{R}_{\alpha'}e^{i\mathbf{p}\cdot\mathbf{R}_{\alpha'}}g(\alpha\,|\,\alpha')B_{LL'}(\alpha\,|\,\alpha')\ , \tag{22c}$$

$$\begin{aligned}B_{LL'}(\alpha\,|\,\beta)=&-4i\pi k(1-\delta_{\lambda0}\delta_{\lambda'0})\\&\times\sum_{J_1}i^{j-j'-j_1}C_{LL'}^{J_1}\\&\times h_{j_1}(k\,|\,\mathbf{R}_\alpha-\mathbf{R}_\beta\,|\,)Y_{J_1}^*(\mathbf{R}_\alpha-\mathbf{R}_\beta)\ ,\end{aligned} \tag{22d}$$

$$C_{LL'}^{J_1}=\int[\mathbf{Y}_L^*(\hat{\mathbf{R}})\cdot\mathbf{Y}_{L'}(\hat{\mathbf{R}})]Y_{J_1}(\hat{\mathbf{R}})d\Omega_{\hat{\mathbf{R}}}\ , \tag{22e}$$

and $h_{j_1}(x)$ is the spherical Hankel function. The Gaunt coefficient $C_{LL'}^{J_1}$ provides constraints on the allowed J_1 values for any L and L'. For all λ values, $j+j'\geq j_1\geq|j-j'|$ and $m=m'+m_1$. The coupling between the λ values provide the additional constraints: For $\lambda=\lambda'$, $j+j'+j_1$ is even, and for $\lambda\neq\lambda'$, $j+j'+j_1$ is odd. The form of $B_{LL'}$ prevents $\lambda=0$ from contributing to Q^{ee}, Q^{em}, Q^{me}, or Q^{mm}, and so $\lambda=0$ is eliminated from the problem.

In the EMA, $\widetilde{B}_{LL'}$ and T_l are defined by

$$\widetilde{B}_{LL'}(\mathbf{p})=B_{LL'}(\mathbf{p})+\sum_{L_1}\frac{1}{n}\int\frac{d\mathbf{p}_1}{(2\pi)^3}h(|\mathbf{p}-\mathbf{p}_1|)\times T_l^{-1}T_{LL_1}(\mathbf{p}_1)\widetilde{B}_{L_1L'}(\mathbf{p}_1)\ , \tag{23a}$$

where $h(|\mathbf{p}|)$ is the Fourier transform of $h(\alpha\,|\,\alpha')$, and

$$T_l(p_1,p_2)=t_l(p_1,p_2)+t_l(p_1,k)f_l(k)t_l(k,p_2)\ . \tag{23b}$$

Of the various forms in which the equation defining $f_l(k)$ can be written, the most convenient for computation is

$$f_l=\sum_{L_1}\frac{1}{n\tau_l}\int\frac{d\mathbf{p}_1}{(2\pi)^3}B_{LL_1}(\mathbf{p}_1)\{T_{L_1L}(\mathbf{p}_1)-T_{l_1}[\widetilde{B}_{L_1L}(\mathbf{p}_1)-B_{L_1L}(\mathbf{p}_1)]T_l\}$$
$$-\sum_{L_1}\frac{n}{\tau_l}\int d\mathbf{R}_{\alpha_1}g(\alpha\,|\,\alpha_1)h(\alpha\,|\,\alpha_1)B_{LL_1}(\alpha\,|\,\alpha_1)T_{l_1}B_{L_1L}(\alpha_1\,|\,\alpha)T_l\ , \tag{23c}$$

where $\tau_l=t_l(k,k)$. The angular integrals eliminate the elements of f which are off diagonal in λ. That f is diagonal in λ immediately implies that the renormalized single-site scattering operator T is diagonal in λ and can be treated as a vector (rather than a dyad).

To find $\epsilon_{\text{eff}}(\omega)$ we numerically, self-consistently solve for T_l and $\widetilde{B}_{LL'}(\mathbf{p})$. Finding the poles of $T(p)$ consists of looking for a zero in the determinant of $1-T_l\widetilde{B}_{LL'}(p\hat{\mathbf{z}})$. Only terms with azimuthal indices $m=\pm1$ contribute to the transverse solution. Since $\widetilde{B}$ is diagonal in its azimuthal indices, and invariant under the transformation $m\rightarrow -m$, it follows that the $m=1$ and -1 blocks of the determinant are identical and we can limit our attention to just one of these blocks. To calculate $\Sigma(p)$ we use T_l and $\widetilde{B}_{LL'}(p\hat{\mathbf{z}})$ along with Eqs. (11), (20), and (21). To obtain the transverse Σ, we again only need the $m=1$ component of $\widetilde{B}(\mathbf{p})$.

D. Long-wavelength limit

1. *Static considerations*

As we pointed out in the Introduction, the standard treatments of the long-wavelength susceptibility in composite media involve two related approximations: (1) only dipole scattering is included, and (2) only the lowest-order density-correlation function (i.e., the packing fraction η) enters the theory. The fact that a proper description of the static dielectric function must involve multipoles of *all* orders has been discussed in several recent papers.[11,13,28] In this subsection we will show how higher-order distribution functions enter the calculation of $\epsilon_{\text{eff}}(\omega=0)$. The essential point is that these quantities are involved in the description of *fluctuations* in the local fields. In the following subsection we will see that such fluctuations are neglected in the QCA but are included approximately by the EMA. In addition, it will be seen that these fluctuation terms couple to the higher multipoles.

To keep the equations as simple as possible, let us work within the dipole approximation. Standard derivations of the ATA equation begin with an array of (spherical) polarizable objects, each of which satisfies[23]

$$\mathbf{p}_i=\frac{\epsilon_s-\epsilon_0}{\epsilon_s+2\epsilon_0}R^3(\mathbf{E}+\mathbf{E}_i)\equiv\gamma(\mathbf{E}+\mathbf{E}_i)\ . \tag{24}$$

Here, $\mathbf{p}_i$ is the induced dipole moment, $\mathbf{E}$ is the macroscopic electric field, $\mathbf{E}_i$ is the local field acting in the ith dipole, and γ is the polarizability of a sphere of radius R.[23] In introducing the local field, the average polarization field $\mathbf{E}_P$ associated with a large sphere (centered at $\mathbf{R}_i$) is subtracted out and the dipoles within the sphere are treated exactly:

$$\mathbf{E}_i\equiv\mathbf{E}_{\text{near}}-\mathbf{E}_P=\mathbf{E}_{\text{near}}+\frac{4\pi}{3}\mathbf{P}\ . \tag{25}$$

The expression for $\mathbf{E}_{\text{near}}$ is

$$\mathbf{E}_{\text{near}}=\sum_{j\neq i}\frac{(3\mathbf{R}_{ij}\mathbf{R}_{ij}-R_{ij}^2\overleftrightarrow{\mathbb{1}})\cdot\mathbf{p}_j}{R_{ij}^5}$$
$$\equiv\sum_{j\neq i}\overleftrightarrow{\Lambda}(\mathbf{R}_{ij})\cdot\mathbf{p}_j\ , \tag{26}$$

where the sum extends over all dipoles within the sphere. Clearly, $\mathbf{E}_{\text{near}}$ depends on the local enviornment of the ith dipole. To derive the ATA one must argue that its contribution can be neglected. This assumption is usually based on the neglect of fluctuations:

$$\mathbf{E}_{\text{near}}\rightarrow\langle\mathbf{E}_{\text{near}}\rangle=\left\langle\sum_{j\neq i}\overleftrightarrow{\Lambda}(\mathbf{R}_{ij})\cdot\mathbf{p}_j\right\rangle$$
$$\rightarrow\left\langle\sum_{j\neq i}\overleftrightarrow{\Lambda}(\mathbf{R}_{ij})\right\rangle\cdot\langle\mathbf{p}_j\rangle\ . \tag{27}$$

Once this assumption is made, the symmetry of the tensor $\overleftrightarrow{\Lambda}(\mathbf{R}_{ij})$ guarantees that the final sum in Eq. (27) vanishes. Combining Eqs. (24), (25), and (27), we find that the average polarization $\mathbf{P}$ is given by

$$\mathbf{P}=n\langle\mathbf{p}\rangle=\frac{n\gamma}{1-(4\pi/3)n\gamma}\mathbf{E}\equiv\chi_0\mathbf{E}\ . \tag{28}$$

[The ATA susceptibility χ_0 and the dielectric function of Eq. (2) are related by $\epsilon=1+4\pi\chi_0$.] More generally, the equations determining the local polarization are

$$\mathbf{p}_i=\gamma\left[\mathbf{E}+\frac{4\pi}{3}\mathbf{P}\right]+\gamma\sum_{j\neq i}\overleftrightarrow{\Lambda}_{ij}\cdot\mathbf{p}_j$$

$$=\gamma\left[1+\gamma\sum_{j\neq i}\overleftrightarrow{\Lambda}_{ij}+\gamma^2\sum_{\substack{j\neq i\\k\neq j}}\overleftrightarrow{\Lambda}_{ij}\cdot\overleftrightarrow{\Lambda}_{jk}+\gamma^3\sum_{\substack{j\neq i\\k\neq j\\l\neq k}}\overleftrightarrow{\Lambda}_{ij}\cdot\overleftrightarrow{\Lambda}_{jk}\cdot\overleftrightarrow{\Lambda}_{kl}+\cdots\right]\cdot\left[\mathbf{E}+\frac{4\pi}{3}\mathbf{P}\right]. \tag{29}$$

Note that the structure of this expansion is quite similar to that of the multiple-scattering series (10). The various terms in the large square brackets of Eq. (29) must be averaged over the different configurations of the neighboring dipoles. The contribution of the two-site term can be evaluated exactly in terms of $g(R)$, and we find

$$\left\langle\sum_{j\neq i}\overleftrightarrow{\Lambda}_{ij}\right\rangle=\int d\mathbf{R}_j\,\overleftrightarrow{\Lambda}_{ij}g(i\,|\,j)=\overleftrightarrow{0}\,. \tag{30}$$

[The vanishing of this term is often used as a justification for the approximation (27).] Note, however, that the contribution due to the third-order term does not vanish:

$$\left\langle\sum_{j\neq i}\sum_{k\neq j}\overleftrightarrow{\Lambda}_{ij}\cdot\overleftrightarrow{\Lambda}_{jk}\right\rangle=\left\langle\sum_{j\neq i}\overleftrightarrow{\Lambda}_{ij}\cdot\overleftrightarrow{\Lambda}_{ji}\right\rangle+\left\langle\sum_{j\neq i}\sum_{k\neq j,i}\overleftrightarrow{\Lambda}_{ij}\cdot\overleftrightarrow{\Lambda}_{jk}\right\rangle$$

$$=\int d\mathbf{R}_j\,g(i\,|\,j)\overleftrightarrow{\Lambda}_{ij}\cdot\overleftrightarrow{\Lambda}_{ji}+\int d\mathbf{R}_j\,d\mathbf{R}_k\,g(i\,|\,j\,|\,k)\overleftrightarrow{\Lambda}_{ij}\cdot\overleftrightarrow{\Lambda}_{jk}\,. \tag{31}$$

Here we have written separately those terms that involve the average positions of two and three sites. Note the similarity of these terms and the fluctuation term considered in Eq. (19). Suppose we write, schematically,

$$\left\langle\sum_{i\neq j}\overleftrightarrow{\Lambda}_{ij}\cdot\mathbf{p}_j\right\rangle\equiv\lambda\mathbf{P}\,, \tag{32}$$

where the parameter λ monitors the influence of the local-field fluctuations. Then the resulting expression for the susceptibility is

$$\mathbf{P}=\frac{n\gamma}{1-(4\pi/3)n\gamma-n\lambda\gamma}\mathbf{E}\equiv\frac{\chi_0}{1-\lambda\chi_0}\mathbf{E}\equiv\chi\mathbf{E}\,. \tag{33}$$

In other words, λ can be viewed as leading to an enhancement of the susceptibility over the ATA value given by χ_0. It is clear from Eqs. (31) that the leading contributions (in powers of γ) to λ can be calculated in terms of the two- and three-site distribution functions.

2. *kd → 0 limit of multiple-scattering theory*

On physical grounds we expect that the effects described above can be understood in terms of the long-wavelength limit of the *dynamic* multiple-scattering equations discussed in Secs. II A–II C. It is clear from Eqs. (21) that, over the entire frequency range, the spectrum is obtained by solving an equation of the form

$$||1-T\widetilde{B}(\mathbf{p})||=0\,, \tag{34}$$

where the determinant refers to (implicit) partial-wave indices.[28] In the long-wavelength limit the analysis of this determinant is complicated by the fact that T_l vanishes as $kd\to0$ while $\widetilde{B}_{LL'}(\mathbf{p})$ diverges.[28] Care must be taken to keep all contributions of order unity in the $kd\to0$ expansion of the (matrix) product $T\widetilde{B}(\mathbf{p})$.

Consider first the QCA [$T\to\tau$ and $\widetilde{B}(\mathbf{p})\to B(\mathbf{p})$]. As $kd\to0$, the dipole components of τ behave as

$$\tau_{e1}=d\left[\frac{\epsilon_s-\epsilon_0}{\epsilon_s+2\epsilon_0}\right]\frac{(kd)^2}{24},\quad \tau_{m1}\sim d(kd)^4\,, \tag{35a}$$

while for higher j we have

$$\tau_{ej}\sim d\left[\frac{\epsilon_s-\epsilon_0}{\epsilon_s+(j+1)\epsilon_0}\right](kd)^{2j},\quad \tau_{mj}\sim d(kd)^{2j+2}\,. \tag{35b}$$

The expression for $B_{LL'}(\mathbf{p})$ [defined by Eq. (22c)] is

$$B_{LL'}(\mathbf{p})=\sum_{J_1}i^{j_1}C^{J_1}_{LL'}B_{j_1}(\mathbf{p})Y^*_{J_1}(\hat{p})\,, \tag{36a}$$

where, as $kd\to0$, and $pd\to0$,

$$B_{j_1}(\mathbf{p})\sim\frac{1}{a}\frac{1}{p^2-k^2}\left[\frac{p}{k}\right]^{j_1}+\int_\sigma^\infty dR\,R^2j_{j_1}(pR)h_{j_1}(kR)h(R)\,. \tag{36b}$$

Here, $j_{j_1}(x)$ is a spherical Bessel function and σ is the effective "hard-sphere" diameter [i.e., $g(R\leq\sigma)=0$]. Since $B(\mathbf{p})\sim1/k^2$ *for all* j, it is clear that the only components of τ that contribute to the determinant $||1-\tau B(\mathbf{p})||$ are those which do not approach zero faster than k^2. The only such component is the electric dipole ($\lambda=e$, $j=1$). The surviving term of $B(\mathbf{p})$ does not involve $g(R)$, and so the resulting $\epsilon_{\text{eff}}(\omega)$ will be *independent* of $g(R)$. It is easily shown that evaluation of the QCA determinant $||1-\tau B(\mathbf{p})||$ gives the ATA result of Eq. (1) or (28). This solution ignores all higher-multipole and local-environment effects.

Turning to the $kd\to0$ limit of the EMA, we find that the coupling between the e and m components of the matrix $\widetilde{B}(\mathbf{p})$ guarantees that magnetic terms drop out as $kd\to0$ and the problem is essentially scalar. The leading contribution to $\widetilde{B}(\mathbf{p})$ is

$$\tilde{B}_{LL'}(\mathbf{p})=B_{LL'}(\mathbf{p})+\delta_{LL'}\sum_{L_1}\frac{1}{n}\int\frac{d\mathbf{p}_1}{(2\pi)^3}h(|\mathbf{p}_1|)T_l^{-1}T_{LL_1}(\mathbf{p}_1)\tilde{B}_{L_1L}(\mathbf{p}_1)\ . \tag{37}$$

Note that the second term on the right-hand side is diagonal in L and independent of $\mathbf{p}$. [As $h(R)$ is nonzero only for $R<R_0$, where R_0 is of order a few grain diameters, the dependence on $\mathbf{p}$ in Eq. (23a) disappears.] There are contributions that are off diagonal in L, but these vanish as $kd\to 0$ and do not couple to the dipole term. Thus in the EMA, as in the QCA, the spectrum is calculated from just the $j=1$ part of the determinant in Eq. (34). However, in the present case higher multipoles contribute through the renormalization of T_l and $\tilde{B}(\mathbf{p})$. (In the Appendix we show that the effect of the jth multipole is scaled down by a factor of roughly $1/4^j$, so that we are dealing with a convergent expansion.)

To make contact with the results of the first part of this subsection, let us expand $\tilde{B}(\mathbf{p})$ and T in powers of η and τ:

$$T_{e1}\approx\tau_{e1}+\tau_{e1}\sum_{j,m}n\int d\mathbf{R}\,g(R)B_{e11,ejm}(\mathbf{R})\tau_{ej}B_{ejm,e11}(-\mathbf{R})\tau_{e1} \tag{38a}$$

and

$$\tilde{B}_{e11,e11}(\mathbf{p})\approx B_{e11,e11}(\mathbf{p})+\sum_{j,m}n^2\int d\mathbf{R}\,d\mathbf{R}_1\,h(|\mathbf{R}-\mathbf{R}_1|)g(R)B_{e11,ejm}(\mathbf{R})\tau_{ej}g(R_1)B_{ejm,e11}(\mathbf{R}_1)\ . \tag{38b}$$

Note that both terms involve $g(R)$ and a sum over internal angular indices. Using Eqs. (35) and (36), we find that Eqs. (38) can be rewritten as

$$T_{e1}=\frac{2}{3}k^2a^3\left[\frac{\epsilon_s-\epsilon_0}{\epsilon_s+2\epsilon_0}\right]\left[1-\eta\left[\frac{\epsilon_s-\epsilon_0}{\epsilon_s+2\epsilon_0}\right]\sum_j\frac{\epsilon_s-\epsilon_0}{(j+1)\epsilon_0+j\epsilon_s}\tilde{a}_j\right] \tag{39a}$$

and

$$\tilde{B}_{e11,e11}(\mathbf{p})=\frac{4\pi n}{p^2-k^2}\left[1+\frac{1}{2}\frac{p^2}{k^2}\right]-\frac{4\pi n}{k^2}\eta\sum_j\left[\frac{\epsilon_s-\epsilon_0}{(j+1)\epsilon_0+j\epsilon_s}\right]\tilde{b}_j\ . \tag{39b}$$

Here, $\tilde{a}_j$ and $\tilde{b}_j$ are geometrical parameters given by

$$\tilde{a}_j\sim\left[\frac{a}{\sigma}\right]^{2j+1}\int dx\,\frac{g(\sigma x)}{x^{2j+2}} \tag{40a}$$

and

$$\tilde{b}_j\sim\left[\frac{a}{\sigma}\right]^{2j-2}\int d\mathbf{x}\,d\mathbf{x}_1\,h(\sigma|\mathbf{x}-\mathbf{x}_1|)F(\mathbf{x})F(\mathbf{x}_1)\ , \tag{40b}$$

where

$$F(\mathbf{x})=\frac{g(\sigma x)}{x^{j+2}}Y^*_{j+1,m-1}(\hat{x}) \tag{40c}$$

and we have neglected all factors of order 1 or j. If we restrict ourselves to $j=1$ we can write ϵ_{EMA} to third order in $(\epsilon_s-\epsilon_0)$ as

$$\epsilon_{\mathrm{EMA}}=1+\frac{3\eta[(\epsilon_s-\epsilon_0)/(\epsilon_s+2\epsilon_0)]}{1-\eta[(\epsilon_s-\epsilon_0)/(\epsilon_s+2\epsilon_0)]}-3\eta^2\left[\frac{\epsilon_s-\epsilon_0}{\epsilon_s+2\epsilon_0}\right]^3(\tilde{a}_1+2\eta\tilde{b}_1)\ . \tag{41}$$

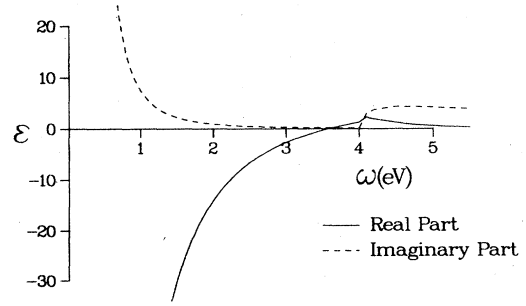

FIG. 1. Real and imaginary parts of the Ag dielectric function used in the Ag-KCl calculation are shown as a function of the frequency (eV). The discontinuity at 4 eV in the real part is due to the mismatch in the models of the dielectric function above and below 4 eV.

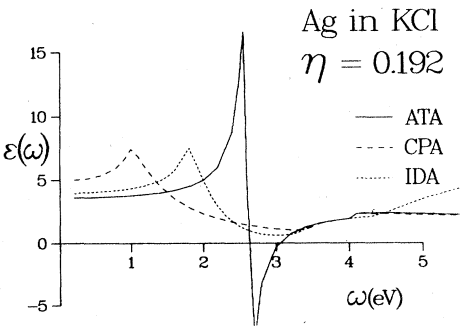

FIG. 2. Real parts of the ATA, CPA, and IDA dielectric functions for Ag spheres in KCl ($\eta=0.192$).

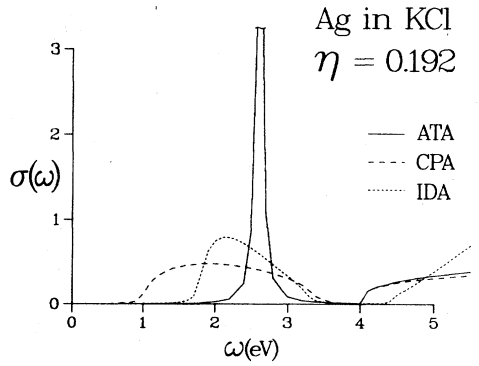

FIG. 3. ATA, CPA, and IDA conductivities for Ag spheres embedded in KCl ($\eta=0.192$).

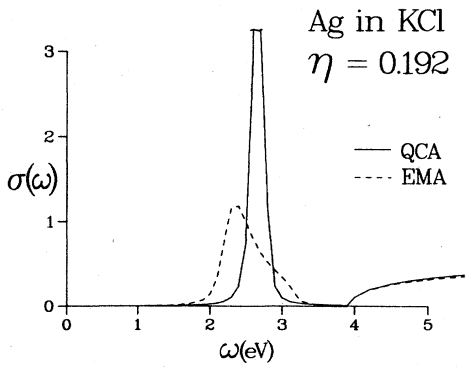

FIG. 5. QCA and EMA conductivities for Ag spheres in KCl ($\eta=0.192$).

This correction is consistent with the form predicted by Eq. (33). Here, however, the three-particle distribution is approximated by the Kirkwood product of three two-particle distributions [recall Eq. (38b)]. Thus, as $kd\rightarrow 0$, the EMA yields results that include correlation effects in a physically reasonable way. Equations (39)—(41) are related to the equations presented in Sec. 5 of Ref. 9. There, Hori and Yonezawa show how cumulant averages that describe short-range correlations lead to corrections to the effective conductivity of a disordered system.[31]

III. CALCULATIONS

A. Metal spheres

To examine the behavior of the QCA and EMA, we first considered a system of silver spheres embedded in the dielectric KCl. Many experiments have been carried out with metal-insulator composites of this kind.[2–6,8] Because these systems have a strong absorption band in the visible, they are promising candidates for use on the absorbing surface of solar cells. The experiments provide a range of results for the position, strength, and shape of the plasmon[2–6,8] resonance. This variation reflects the fact that the composites are not always synthesized in a way that guarantees a suspension geometry. However, in the cases where the metal particles are known to be nonoverlapping, the data suggest that the plasmon resonance is appreciably broader and is shifted to lower frequencies than the resonance predicted by the ATA.[3–6,16]

We have studied the effective dielectric function for a suspension of Ag spheres of radius 120 Å in a KCl host ($\epsilon_0=2.1$) with a packing fraction of $\eta=0.192$. (The input data for this calculation correspond to one of the systems considered in Ref. 8.) The dielectric function of the spheres was modeled using a combination of the Drude model (frequencies below 4 eV) and experimental data[32] (frequencies above 4 eV) in order to include the effects of the interband transitions. The Drude formula is

$$\epsilon_s(\omega)=\epsilon_b-\frac{\omega_p^2}{\omega^2-i\omega/\tau}\ . \tag{42}$$

To model silver, we used $\epsilon_b=6.4$, $\omega_p=9.06$ eV, and $1/\tau=0.0918$ eV. The value for τ is greater than the bulk value in order to include the effects of scattering from the surface of the sphere. Figure 1 shows the Ag dielectric function. Unfortunately, in the real part of this function the segment obtained from the experimental data does not join smoothly with the segment obtained from the Drude model. This small jump will cause a similar jump in the calculated effective dielectric function of the suspension,

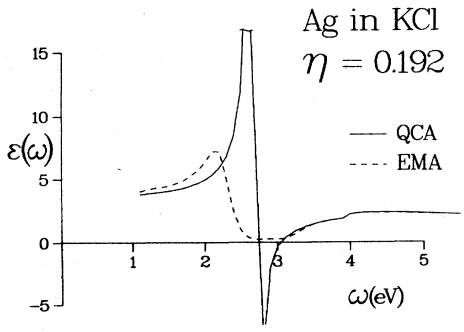

FIG. 4. Real parts of the QCA and EMA dielectric functions for Ag spheres embedded in KCl ($\eta=0.192$).

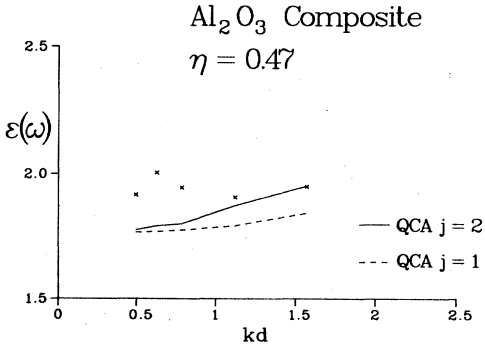

FIG. 6. QCA dielectric function for the Al_2O_3 composite with $\eta=0.47$ compared with experiment (Ref. 7). Calculations with $j_{max}=1$ and 2 are shown.

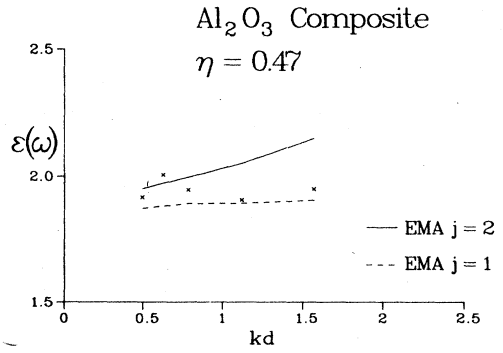

FIG. 7. EMA dielectric function for the Al_2O_3 composite with $\eta=0.47$ compared with experiment (Ref. 7). Calculations with $j_{max}=1$ and 2 are shown.

but as the resonance is significantly below 4 eV it does not interfere with the resonance position or shape.

In Figs. 2 and 3 calculations based on the ATA, CPA, and IDA for this system are compared. The ATA shows very strong resonance behavior in a narrow frequency range, while the CPA shows a weak resonance shifted very far to the left. The IDA predicts a resonance with a position and shape roughly intermediate between the ATA and CPA results. Of the three, the IDA results are closest to those of the experiments, but the shift appears to be too large and the shape of the curves does not match well.[33]

Our results for the frequency dependence of the dielectric function and conductivity of the suspension are shown in Figs. 4 and 5. The QCA results are very similar to the ATA results, as expected for longer-wavelength calculations. The QCA peak in $\sigma(\omega)$ is slightly broadened and shifted to higher frequencies. The shift is much smaller than the experimentally observed shift and is in the wrong direction. By contrast, the EMA peak in $\sigma(\omega)$ is significantly broadened and shifted to the left and is, in fact, quite similar to the relevant experimental results.[3,8,16] The shape of the EMA peak is also similar to

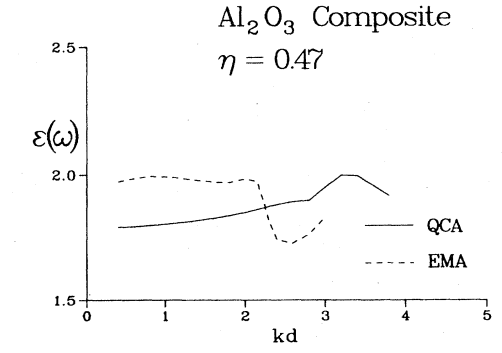

FIG. 8. QCA and EMA dielectric functions for the Al_2O_3 composite with $j_{max}=2$, $\eta=0.47$, and $\epsilon_s=3.4$ (frequency independent).

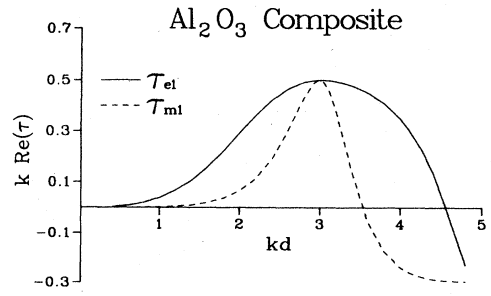

FIG. 9. Real part of $k\tau$ for $j=1$ shown as a function of frequency.

that of the measured peak, being somewhat broader on the higher-frequency side.

B. Al_2O_3 pressed powder

The second system we examined is a suspension of Al_2O_3 spheres in air where the Al_2O_3 forms a volume fraction of 0.47 of the suspension. Our results are compared with experimental data taken by Egan and Aspnes.[7] Their system was a compressed powder of Al_2O_3 formed into pellets, so it is not clear how well our calculations model the microgeometry of their samples. We show the results of QCA and EMA calculations compared with the experimental data in Figs. 6 and 7. For these calculations the measured values for the dielectric function of Al_2O_3 given in Ref. 7 were employed. The experimental data for the composite have a great deal of scatter, so it is difficult to draw unambiguous conclusions as to the level of agreement between theory and experiment.

In the light of the discussion in Sec. II D, this system is of interest because it allows us to compare the behavior of QCA and EMA calculations with different values of j_{max}. Figure 6 shows that for the smaller kd values the QCA results for a calculation where only $j=1$ is included are not very different from the results when both $j=1$ and 2 are employed. By contrast, Fig. 7 shows that $j=2$ does significantly contribute to the EMA results, even for the longest wavelength. We believe that these are the first

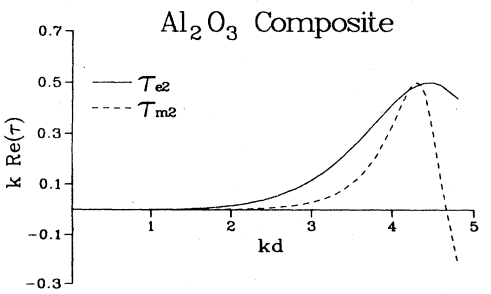

FIG. 10. Real part of $k\tau$ for $j=2$ shown as a function of frequency.

calculations which show the influence of higher multipoles in calculating the long-wavelength dielectric properties of disordered suspensions.

In order to isolate the effects of the frequency dependence of the Al_2O_3 dielectric function from the effects of the changing wavelength to sphere-size ratio, we repeated our calculations using a constant dielectric function of $\epsilon_s=3.4$. The results with $j_{\max}=2$ are shown in Fig. 8. At least some of the structure above $kd=2.2$ appears to be due to rapid changes in the $l=m1$ component of τ. In Figs. 9 and 10 we show how the real part of τ varies with frequency for $j=1$ and 2. Note that the structure in τ appears at higher frequencies than the corresponding structure in $\epsilon_{\text{eff}}(\omega)$. This shift may be analogous to the shift in the resonance position found in the Ag-KCl composite.

ACKNOWLEDGMENTS

We would like to thank D. Johnson for several important conversations. We are grateful to D. Stroud and W. Chew for discussions in the early stages of this work. K. Cummins and D. Tanner provided us with data on the dielectric function for Ag grains. One of us (V.A.D.) would like to acknowledge support from the National Science Foundation and from Schlumberger-Doll Research.

APPENDIX

Here we estimate the contribution of higher multipoles to the EMA correction to $B(\mathbf{p})$ and τ in the long-wavelength limit. All multipoles contribute even at long wavelengths, but as we show below the terms for the higher multipoles decrease by a factor of roughly $1/4^j$. To provide an estimate of how the coefficient decreases, we examine only the first-order correction:

$$\widetilde{B}_{e\,11,e\,11}(\mathbf{p})-B_{e\,11,e\,11}(\mathbf{p})=\sum_{j,m}\frac{1}{n}\int\frac{d\mathbf{p}_1}{(2\pi)^3}h(p_1)B_{e\,11,ejm}(\mathbf{p}_1)\tau_{ej}B_{ejm,e\,11}(\mathbf{p}_1) \tag{A1a}$$

and

$$f^{e\,1}=\sum_{j,m}n\int d\mathbf{R}\,g(R)B_{e\,11,ejm}(\mathbf{R})\tau_{ej}B_{ejm,e\,11}(-\mathbf{R})\ , \tag{A1b}$$

where f is written as a real-space integral for clarity. In the long-wavelength limit we have

$$B_{e\,11,ejm}(\mathbf{R})=4\pi k(-1)^j\frac{1\times3\times5\times\cdots\times(2j+1)}{(kR)^{j+2}}C^{j+1,m-1}_{e\,11,ejm}Y^*_{j+1,m-1}(\hat{\mathbf{R}})\ , \tag{A2a}$$

$$B_{e\,11,ejm}(\mathbf{p}_1)=i^jk(4\pi)^2C^{j+1,1-m}_{e\,11,ejm}Y^*_{j+1,1-m}(\hat{\mathbf{p}}_1)n\sigma^3\frac{1\times3\times5\times\cdots\times(2j+1)}{(k\sigma)^{j+2}}F(p_1)\ , \tag{A2b}$$

where

$$F(p_1)=\frac{j_j(p_1\sigma)}{p_1\sigma}+\int_1^\infty dx\frac{j_{j+1}(p_1\sigma x)h(\sigma x)}{x^j}$$

and

$$\tau_{ej}=\frac{1}{k}\frac{(j+1)(ka)^{2j+1}}{[1\times3\times5\times\cdots\times(2j-1)]^2(2j+1)}\left[\frac{\epsilon_s-\epsilon_0}{(j+1)\epsilon_0+j\epsilon_s}\right]\ . \tag{A2c}$$

To estimate the behavior of B, we must understand how

$$C_j\equiv\sum_m\frac{1}{n}\int\frac{d\mathbf{p}_1}{(2\pi)^3}h(p_1)B_{e\,11,ejm}(\mathbf{p}_1)\tau_{ej}B_{ejm,e\,11}(\mathbf{p}_1) \tag{A3}$$

varies with j. The angular integral gives 1 by orthogonality. The integral over p_1 is

$$I_j=\int_0^\infty dp_1\,p_1^2h(p_1)\left[\frac{j_j(p_1\sigma)}{p_1\sigma}+\int_1^\infty dx\frac{j_{j+1}(p_1\sigma x)h(\sigma x)}{x^j}\right]^2\ . \tag{A4}$$

This integral does not have a strong dependence on j, but slightly decreases with increasing j. We estimate the j dependence of the Gaunt factor sum over the azimuthal index to be roughly $2j+1$, as, for each j value, there are $2j+1$ values of m. (This is almost certainly an overestimate, as the larger j values have less overlap between the spherical harmonics in the integrals.) Thus,

$$\sum_m C^{j+1,1-m}_{e\,11,ejm}C^{j+1,m-1}_{ejm,e\,11}\sim2j+1\ , \tag{A5}$$

and the j-dependent part of the correction factor is

$$C_j \sim (2j+1)^2(j+1)\left[\frac{ka}{k\sigma}\right]^{2j}\frac{\epsilon_s-\epsilon_0}{(j+1)\epsilon_0+j\epsilon_s}I_j \ . \tag{A6}$$

where the primary j dependence comes from the a/σ factor. For any close-packed distribution, $a/\sigma=\frac{1}{2}$, and so the overall dependence of the correction varies as $1/4^j$. An analogous calculation shows that corrections to τ_j fall off similarly with increasing j.

[1]*Electrical Transport and Optical Properties in Inhomogeneous Media (Ohio State University, 1977), Proceedings of the First Conference on the Electrical Transport and Optical Properties of Inhomogeneous Media,* edited by J. C. Garland and D. B. Tanner (AIP, New York, 1978).

[2]E. B. Priestley, B. Abeles, and R. W. Cohen, Phys. Rev. B **12**, 2121 (1975).

[3]J. I. Gittlemand and B. Abeles, Phys. Rev. B **15**, 3273 (1977).

[4]U. Kreibig, Z. Phys. B **31**, 39 (1978).

[5]C. G. Granqvist, J. Appl. Phys. **50**, 2916 (1979).

[6]U. Kreibig, A. Althoff, and H. Pressmann, Surf. Sci. **106**, 308 (1981).

[7]W. G. Egan and D. E. Aspnes, Phys. Rev. B **26**, 5313 (1982).

[8]K. D. Cummings, J. C. Garland, and D. B. Tanner, in *Physics and Chemistry of Porous Media (Schlumberger-Doll Research),* edited by D. L. Johnson and P. N. Sen (AIP, New York, 1984), p. 38; Phys. Rev. B **30**, 4170 (1984).

[9]M. Hori and F. Yonezawa, J. Phys. C **10**, 229 (1977).

[10]D. Stroud and F. P. Pan, Phys. Rev. B **17**, 1602 (1978).

[11]D. R. McKenzie and R. C. McPhedran, Nature (London) **265**, 129 (1977); R. C. McPhedran and D. R. McKenzie, Proc. R. Soc. London, Ser. A **359**, 45 (1978).

[12]V. K. Varadan, V. N. Bringi, and V. V. Varadan, Phys. Rev. D **19**, 2480 (1979); V. V. Varadan and V. K. Varadan, *ibid.* **21**, 388 (1980).

[13]W. Lamb, D. M. Wood, and N. W. Ashcroft, Phys. Rev. B **21**, 2248 (1980).

[14]L. Tsang and J. A. Kong, J. Appl. Phys. **51**, 3465 (1980); **53**, 7162 (1982).

[15]D. J. Bergman and D. Stroud, Phys. Rev. B **22**, 3527 (1980).

[16]B. N. J. Persson and A. Liebsch, Solid State Commun. **44**, 1637 (1982); A. Liebsch and B. N. J. Persson, J. Phys. C **16**, 5375 (1983); A. Liebsch and P. Villaseñor González, Phys. Rev. B **29**, 6907 (1984).

[17]V. Twersky, J. Opt. Soc. Am. **73**, 1562 (1983).

[18]G. S. Agarwal and R. Inguva, Phys. Rev. B **30**, 6108 (1984).

[19]As noted above, if all the inclusions are spheres of the same radius, the packing fraction is limited to $\eta \lesssim 0.62$. To obtain higher values of η, the model must be generalized to include either spheres of varying radii or grains that the nonspherical in shape.

[20]J. C. Maxwell Garnett, Philos. Trans. R. Soc. London **203**, 385 (1904).

[21]D. A. G. Bruggeman, Ann. Phys. (Leipzig) **24**, 636 (1935).

[22]P. N. Sen, C. Scala, and M. H. Cohen, Geophysics **46**, 781 (1981).

[23]J. D. Jackson, *Classical Electrodynamics,* 2nd ed. (Wiley, New York, 1975), Sec. 4.5.

[24]M. Lax, Rev. Mod. Phys. **23**, 287 (1951).

[25]L. Roth, Phys. Rev. B **9**, 2476 (1974).

[26]L. Huisman, D. Nicholson, L. Schwartz, and A. Bansil, Phys. Rev. B **24**, 1824 (1981).

[27]L. Schwartz and T. J. Plona, J. Appl. Phys. **55**, 3971 (1984).

[28]Within the framework of long-wavelength acoustic propagation, the application of the EMA to ordered and disordered suspensions is discussed by L. M. Schwartz and D. L. Johnson [Phys. Rev. B **30**, 4302 (1984)].

[29]Because the average system is translationally invariant and isotropic all of the dyads discussed in Sec. IIA can be written in terms of their longitudinal and transverse projections. For example,

$$\vec{\mathbf{G}}(\mathbf{p})=G_{||}(p)\hat{\mathbf{p}}\hat{\mathbf{p}}+G_{\perp}(p)(\vec{\mathbb{1}}-\hat{\mathbf{p}}\hat{\mathbf{p}})$$

$$=[k^2-\Sigma_{||}(p)]^{-1}\hat{\mathbf{p}}\hat{\mathbf{p}}+[k^2-p^2-\Sigma_{\perp}(p)]^{-1}(\vec{\mathbb{1}}-\hat{\mathbf{p}}\hat{\mathbf{p}}) \ .$$

We are, of course, only interested in the propagation of transverse waves.

[30]We use a distribution function taken from experimental studies of liquid metals. Our choice corresponds to molten Cu at $T=1100\,^{\circ}\mathrm{C}$ (see D. Nicholson, A. Chowdhary, and L. Schwartz [Phys. Rev. B **29**, 1633 (1984)]). As a matter of practice, we have found that the detailed shape of $g(R)$ is relatively unimportant as long as this function satisfies the constraints discussed by Nicholson *et al.*

[31]Hori and Yonezawa (Ref. 9) employ a *cumulant approximation* whose formal structure is equivalent to that of the EMA. This equivalence is established in the paper by F. Yonezawa, L. Roth, and M. Watabe [J. Phys. F **5**, 435 (1975)] cited in Ref. 9.

[32]K. D. Cummings and D. Tanner (private communication).

[33]In Figs. 2–5 we have not reproduced the experimental results of Ref. 8 because we are not certain that the method of sample preparation employed therein guarantees that the system studied there has suspension geometry. Indeed, the emphasis in Ref. 8 was the study of the percolation transition that takes place when the metal particles form interconnecting channels through the material. While the $\eta=0.192$ composite was *not* metallic, we are not sure that the Ag particles can realistically be modeled as nonoverlapping spheres in this case.